This is the pre-review version of the paper published in

J. Phys. Chem. B, 114, 8994–9001

The final version may be obtained from the publisher, at the following link

http://pubs.acs.org/articlesonrequest/AOR-65CEnKDdRjmGVubTh5zz

A tale of two acids: when arginine is a more appropriate acid than H_3O^+.

Pedro J. Silva[a‡*] *, Claudia Schulz*[b‡], *Dieter Jahn*[b], *Martina Jahn*[b] *and Maria João Ramos*[c]

[a] REQUIMTE, Fac. de Ciências da Saúde, Univ. Fernando Pessoa, Rua Carlos da Maia, 296, 4200-150 Porto-Portugal

[b] Department of Microbiology,Technische Universitaet Braunschweig, Spielmannstr. 7, 38106 Braunschweig - Germany

[c]REQUIMTE, Faculdade de Ciências do Porto, Rua do Campo Alegre, 687, 4169-007 Porto – Portugal

[‡]These authors contributed equally to this paper.

Abstract:

Uroporphyrinogen III decarboxylase catalyzes the fifth step in heme biosynthesis: the elimination of carboxyl groups from the four acetate side chains of uroporphyrinogen-III to yield coproporphyrinogen-III. We have previously found that the rate-limiting step is substrate protonation, rather than decarboxylation itself, and that this protonation can be effected by a nearby arginine residue (Arg37). In this report, we have studied the reasons for the unusual choice of arginine as a general acid catalyst. Our density functional calculations show that, although substrate protonation by H_3O^+ is both exergonic and very fast, in the presence of a protonated Arg37 substrate decarboxylation becomes rate-limiting and the substrate spontaneously breaks upon protonation. These results suggest that the active site must be shielded from solvent protons, and that therefore H_3O^+ should be excluded from a role in both protonations present in this mechanism. A second Arg residue (Arg41) is uniquely positioned to act as donor of the second proton, with an activation barrier below 2 kcal mol^{-1}. Additional site-directed mutagenesis experiments confirmed that no coproporphyrinogen is formed in the absence of any of these these Arg residues. This counter-intuitive use of two basic residues as general acids in two different proton donation steps by uroporphyrinogen decarboxylase may have arisen as an elegant solution to the problem of simultaneously binding the very negative uroporphyrinogen (which requires a positively charged active site), and selectively protonating it while preventing excessive carboxylate stabilization by positive charges.

KEYWORDS: uroporphyrinogen decarboxylase; reaction mechanism; decarboxylation; density-functional theory; binding/unbinding events

*corresponding author: pedros@ufp.edu.pt

I. Introduction

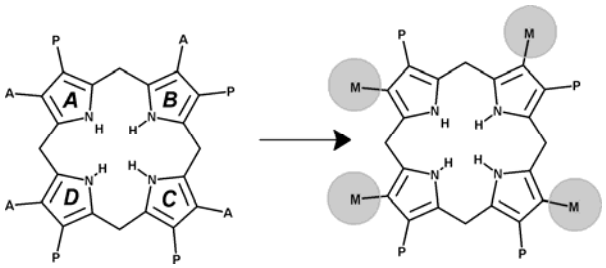

The most common porphyria in humans is porphyria cutanea tarda (PCT), which results from the accumulation of uroporphyrin and partially decarboxylated intermediates in the liver, plasma and skin and is characterized by severe photosensitive dermatosis, hypertrichosis and hyperpigmentation[1]. The origin of the disease has been traced to the impairment of the key enzyme uroporphyrinogen-III decarboxylase (UroD), which catalyzes the fifth step in heme biosynthesis: the elimination of carboxyl groups from the four acetate side chains of uroporphyrinogen-III to yield coporporphyrinogen-III[2]. UroD is quite an unusual decarboxylase, since it performs decarboxylations without the intervention of any cofactors unlike the vast majority of decarboxylases. By adapting an earlier proposal[3], we have recently proposed that protonation of the Asp86-stabilized pyrrole ring by Arg37 will enable it to act as an electron sink, thereby enabling the decarboxylation[4]. A second protonation of the pyrrole ring, followed by the return of the first proton to the original acidic residue yields the desired product (Fig.1). Density-functional calculations on this reaction mechanism are fully consistent[4] with UroD inactivation by the arginine-modifying reagent phenylglyoxal[5] and with the experimental reaction rate[6]. These calculations showed that substrate protonation was the rate-limiting step, and that decarboxylation of the protonated substrate had a very small (8.4 kcal.mol^{-1}) activation free energy.

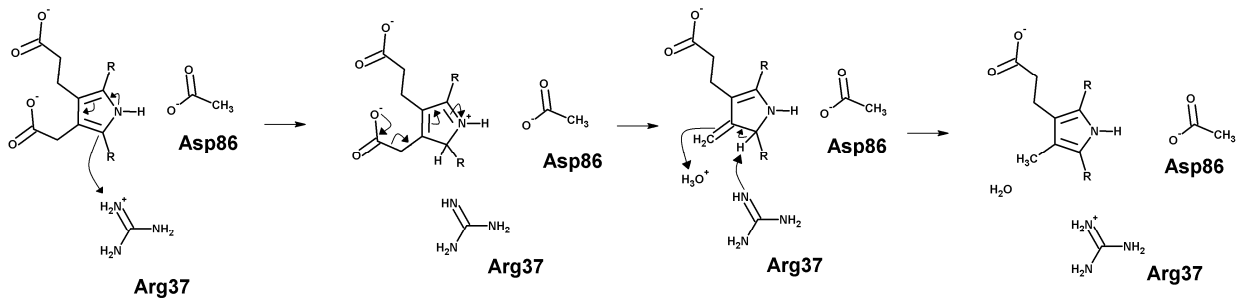

Fig. 1: Proposed reaction mechanism for UroD (adapted from Silva & Ramos, 2005). Since all four pyrrole rings present in the substrate are decarboxylated by UroD, the reaction cycle depicted must be repeated three more times.

With substrate protonation as the rate-limiting, stronger acids should yield faster reaction rates. Such reaction rates do not occur in the enzyme, and it is well known that in strongly acidic conditions H_3O^+ catalyzes uroporphyrinogen decarboxylation at much slower rates than the enzyme-catalyzed reaction[7]. These paradoxes, together with the counter-intuitive use of arginine as an acidic residue, prompted the present study on potential evolutionary shortcomings of the use of the much stronger acid, H_3O^+, as proton donor in the enzymatic reaction.

II. Methods

Quantum chemistry

All calculations were performed at the Becke3LYP level of theory[8,9,10]. In geometry optimizations a medium-sized basis set, 6-31G(d), was used, since it is well known that larger basis sets give very small additional corrections to the geometries, and their use for this end is hence considered unnecessary from a computational point of view[11,12,13]. More accurate energies of the optimized geometries were calculated with the triple-ζ quality basis set 6-311+G(2d,2p). As in our previous work, our calculations focused on the decarboxylation of pyrrole ring D of uroporphyrinogen III, since this is believed to be the first ring to undergo decarboxylation in physiological conditions[14]. Asp86, Arg37 and H_3O^+ were incorporated into the model. Two water molecules were also included, in order to provide some charge stabilization and for added realism. In order to prevent unrealistic movements of the modeled aminoacid sidechains, aminoacid Cα and Cβ carbon atoms were constrained to their crystallographic positions[3].

Likewise, the intervening substrate pyrrole ring D was also anchored to its initial coordinates by freezing two of its carbon atoms. Constraints imposed on the geometries prevented frequency analyses: zero point (ZPE) and thermal effects (T=310.15 K, P=1 bar) were estimated from calculations on smaller unconstrained models: contributions for the proton transfer between H_3O^+ and the substrate were estimated from the proton transfer between solvated H_3O^+ and unsubstituted pyrrole; an estimate for ZPE and thermal effects for the decarboxylation of the protonated substrate was taken from our previous work[4]. A scaling factor of 0.9804 was used for the frequencies.

The polarizable conductor model[15,16], as implemented in Gaussian03[17] was used in order to account for the effects of the protein environment. The dielectric constant was chosen equal to 4, as commonly used for the active site of proteins[18]. Atomic charge and spin density distributions were calculated with a Mulliken population analysis[19], using the larger basis set. All calculations were performed with the Gaussian03 suite of programs.

Continuum electrostatic calculations

In order to characterize the substrate protonation state and the relevant interactions in the enzyme-substrate complex, continuum electrostatic calculations were performed using MEAD[20]. PARSE charges and radii[21] were assigned to the structure of human UroD dimer[22] with one bound substrate molecule using PDB2PQR[23]. The solvent probe radius was 1.4 Å, which should be a reasonable spherical approximation of the water molecule, the ionic exclusion layer thickness was set at 2.0 Å, and temperature at 310 K. The dielectric constant used for the solvent region was 80, the approximate value for bulk water at room temperatures. The dielectric constant for the protein interior was set to 15, the value previously found to yield optimum results with this methodology[24,25]. A two-step focusing method[26] was used: a first calculation using a $(300\ Å)^3$ cube with a 1.0-Å lattice spacing, centered on the protein, followed by a second calculation using a $(75\ Å)^3$ cube with a 0.25-Å spacing, centered on the titrable site; for the model compounds calculations, the sides of the cubes were, respectively, 190 Å

and 47.5 Å. With the exception of Asp86 in the substrate-bound subunit, all Asp, Glu, His, Arg, Lys, Tyr and Cys residues, as well as the substrate acetate and propionate substituents, were allowed to titrate. The sampling of proton-binding states was done using the MCRP program (Monte Carlo for Reduction and Protonation), which implements a Monte Carlo method described by Baptista et al.[27,28]. pH was sampled at 0.2 pH units intervals in the 0-15 range. Occupation states and correlations were computed using 10^6 Monte Carlo steps.

Molecular dynamics

All simulations were run with YASARA[29] with the AMBER99[30] forcefield, using a multiple time step of 1.25 fs for intramolecular and 2.5 fs for intermolecular forces. Simulations were performed in cells 10 Å larger than the protein dimer along each axis (final cell dimensions 108.63 × 82.50 × 72.64 $Å^3$) , and counter-ions were added to a final concentration of 0.9 % NaCl. A 7.86 Å cutoff was taken for Lennard-Jones forces and the direct space portion of the electrostatic forces, which were calculated using the Particle Mesh Ewald method[31] with a grid spacing <1 Å, 4th order B-splines and a tolerance of 10^{-4} for the direct space sum. Simulated annealing minimizations started at 298 K, velocities were scaled down with 0.9 every ten steps for a total time of 5 ps. After annealing, simulations were run at 298 K. Temperature was adjusted using a Berendsen thermostat[32] based on the time-averaged temperature, i.e. to minimize the impact of temperature control, velocities were rescaled only about every 100 simulation steps, whenever the average of the last 100 measured temperatures converged. Energy Substrate parameterization was performed with the AM1BCC protocol[33]. Protein sidechain protonation patterns were assigned according to Krieger *et al.*[34]. Substrate protonation was set according to the results of the continuum electrostatic computations (see below), i.e. propionic acid substituents on rings B and C were kept protonated while all others substituents were deprotonated. The simulations were run for 10 ns after an initial 500 ps equilibration.

Site-directed mutagenesis of the human *hemE* gene

To exchange nucleotides in the human *hemE* gene, the QuikChange®II Site-Directed Mutagenesis Kit (Stratagene, Heidelberg, Germany) was used according to the manufacturer's instructions by using the expression vector pHT#77 as template[35]. Oligonucleotides carrying nucleotide exchanges compared with the *hemE* gene sequence in the underlined positions were used to generate mutants: R37A: 5´-GTTTGGTGCATGGCCCAGGCAGGCCG-3´; R37K: 5´-GTTTGGTGCATGAAACAGGCAGGCCG-3´; R41A: 5´-CGCCAGGCAGGCGCCTACTTACCAGAG-3´; R41K: 5´-CGCCAGGCAGGCAAATACTTACCAGAG-3´. All mutated genes were verified for gene integrity by DNA sequence determination.

Production and purification of Uroporphyrinogen-III-decarboxylase (UroD)

The expression vector pHT#77 carrying the human *hemE* gene and mutant variants were transformed into the *E. coli* strains BL21(DE3)RIL for the mutant variants R37A, R41A, R41K, respectively BL21(DE3)pLysS for the wild type and R37K variant. For protein production 3 litre cultures were grown to an OD_{578} of 0.6 at 37 °C, then induced with 400 µM isopropyl-β-D-thiogalactopyranosid and shifted to 25 °C for 6 h. The cells were harvested by centrifugation and stored at -20 °C. Cells were resuspended in buffer A (300 mM NaCl; 50 mM Sørensen's phosphate buffer (pH 6.8;); 10 % (v/v) glycerol)[36]. Cells were disrupted by a single passage through a French press homogenizer at 19.200 psi. The insoluble cell components were removed by centrifugation for 90 min at 25.000 x g. The supernatant was loaded onto a 5 mL Ni^{2+}- NTA column (HiTrap™Chelating HP; Amersham Biosciences, Uppsala, Sweden) which was equilibrated with buffer A. The column was washed with 50 mL buffer A to remove unbound proteins. Bound proteins were eluted using a linear gradient of 0-250 mM imidazole in buffer A at a flow rate of 0.5 mL/min. Fractions containing UroD were identified by SDS-PAGE. Concentrations of protein solutions were determined using the Bicinchoninic Acid Kit for

Protein Determination (Sigma – Aldrich, Munich, Germany) according to manufacturer's instructions and concentrated by ultrafiltration (vivaspin 15, Vivascience, Hanover, Germany) and stored at 4 °C.

Enzyme activity assay

The UroD activity assay was carried out under strict anaerobic conditions. The reaction components were mixed in an anaerobic chamber. All solutions used were saturated with N_2 prior to use. The standard assay mixture contained UroD (0.1 µM) and uroporphyrinogen-III (0,025 – 20 µM) in potassium phosphate buffer in a total volume of 240 µL after a modified procedure as described earlier[37]. After incubation at 37 °C in the dark for 30 min the reaction was stopped by the addition of 10 µL concentrated HCl and formed coproporphyrinogen-III was oxidised for 15 min to coproporphyrin-III by addition of 10 µL 30 % H_2O_2. The mixture was centrifuged for protein removal for 15 min at 15.000 x g. The obtained supernatant was analysed by High Performance Liquid Chromatography (HPLC). The HPLC system was Jasco 1500 series (Jasco, Gross-Umstadt, Germany). Therefore, 100 µL of the supernatant was mixed with 100 µL acetone/HCl (9:10). Twenty µL were loaded onto a 250 x 4,6 mm Equisil ODS C_{18} reversed phase column (Dr. Maisch GmbH, Ammerbuch, Germany). Separation was performed at a flow rate of 0.3 mL/min using 40 % (v/v) ammoniumacetate (pH 5.2) and 10 % (v/v) acetonitrile in methanole as mobile phase. Tetrapyrroles were detected by fluorescence measurement using an excitation wavelength of 409 nm and an emission wavelength of 618 nm. Uroporphyrin-III and Coproporphyrin-III (Frontier Scientific, Germany, European Union) were used as standards.

III. Results

Since H_3O^+ is a stronger acid than aspartate, in our models H^+ naturally tended to move towards Asp86. This movement (which is opposed in the enzyme by the low concentration of available H_3O^+) could only be prevented in our models by constraining the O-H bonds in the hydronium ion to their equilibrium length (0.9888 Å). The identification of the reactant, transition state and product structures

for proton transfer from H_3O^+ to the pyrrole ring was therefore performed subject to these constraints. We found that initially the reactive proton in H_3O^+ lies 1.92 Å away from the pyrrole C2 atom. Charge stabilization of H_3O^+ is provided by the pyrrole acetate substituent (1.53 Å away) and by a H_2O molecule positioned approximately midway between H_3O^+ and Asp86. In this model, the protonated Arg37 stabilizes the acetate substituent, with one of its Nη1 guanidinium protons positioned 1.70 Å from one of the carboxylate oxygens, and a water molecule providing a bridge between the remaining carboxylate oxygen and the Nη2 guanidinium hydrogens.

Proton transfer from H_3O^+ to the pyrrole ring requires a very small (0.23 Å) movement of the H_3O^+ center of mass. In the transition state (Figure 2a), the H-O distance has increased to 1.26 Å , and the H-pyrrole distance has decreased to 1.37 Å. The original positive charge has partially spread from the H_3O^+ (which retains only +0.68 charge) to the pyrrole (which has acquired +0.32 charge). This step occurs with a very small energetic barrier (3.3 kcal.mol^{-1} electronic energy difference, ΔG=0.3 kcal.mol^{-1}). At pH=6.2, the optimum pH for the human enzyme reaction rate[6], the initial energy of the system should be decreased by a factor of RT ln (H^+), yielding an effective barrier of 8.8 kcal.mol^{-1}. This reaction step is moderately exergonic, as the product lies 11.9 kcal mol^{-1} below the transition state. The protonated pyrrole ring formed in this step is stabilized through interaction with Asp86, and its acetic acid substituent strongly interacts with the protonated Arg37 residue. We computed the energetic contribution of these amino acids by repeating the calculations in their absence, while keeping their orbitals in order to avoid basis step superposition errors. These calculations show that Asp86 and Arg37 together lower the reaction product energy by 9 kcal mol^{-1}.

In the transition state for the decarboxylation step the pyrrole-CO_2 bond has stretched to 2.424 Å, similar to the value previously found for the same reaction with a deprotonated Arg37 (2.48 Å), and a small (-0.131 a.u.) charge on the leaving CO_2 (Figure 2b). However, the strong stabilization of the leaving carboxylate by the *protonated* Arg37 dramatically increases the barrier for decarboxylation from the 8.4 kcal.mol^{-1} computed for a deprotonated Arg37[4] to 18.0 kcal.mol^{-1}. Decarboxylation thus becomes rate-limiting, in contrast to the behavior observed with Arg37 as proton donor. The high

barrier for decarboxylation enables other reaction pathways to become competitive with CO_2 evolution. In particular, breaking of the protonated tetrapyrrole ring now becomes possible: elongation of the C-C bond between C2 of ring D and the methylene bridging rings D and A allowed us to identify a low-lying transition state 12.8 kcal.mol^{-1} above the protonated uroporphyrinogen (Figure 2c). The energy and geometry of this transition state are very similar to those observed in a related reaction performed by uroporphyrinogen III synthase[38], which catalyzes the previous step in heme biosynthesis. It is clear from these calculations that in the presence of a protonated Arg37 substrate degradation occurs faster than decarboxylation, and that the correct reaction product cannot be formed quantitatively. These results show that H_3O^+ entry to the active site is disadvantageous for the enzyme-catalyzed reaction, and provide an interesting explanation for the unusual choice of an arginine residue as general acid in this reaction mechanism.

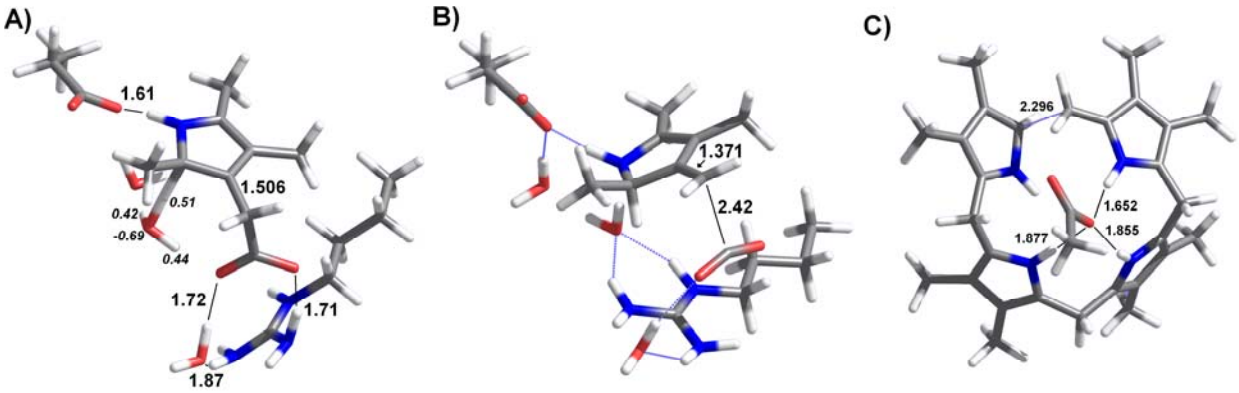

Figure 2: Structures of the transition states for: a) proton transfer from H_3O^+ to the substrate; b) decarboxylation of the protonated substrate; c) breaking of the protonated tetrapyrrole ring. All distances in Å. Relevant charges in italics (in a.u.).

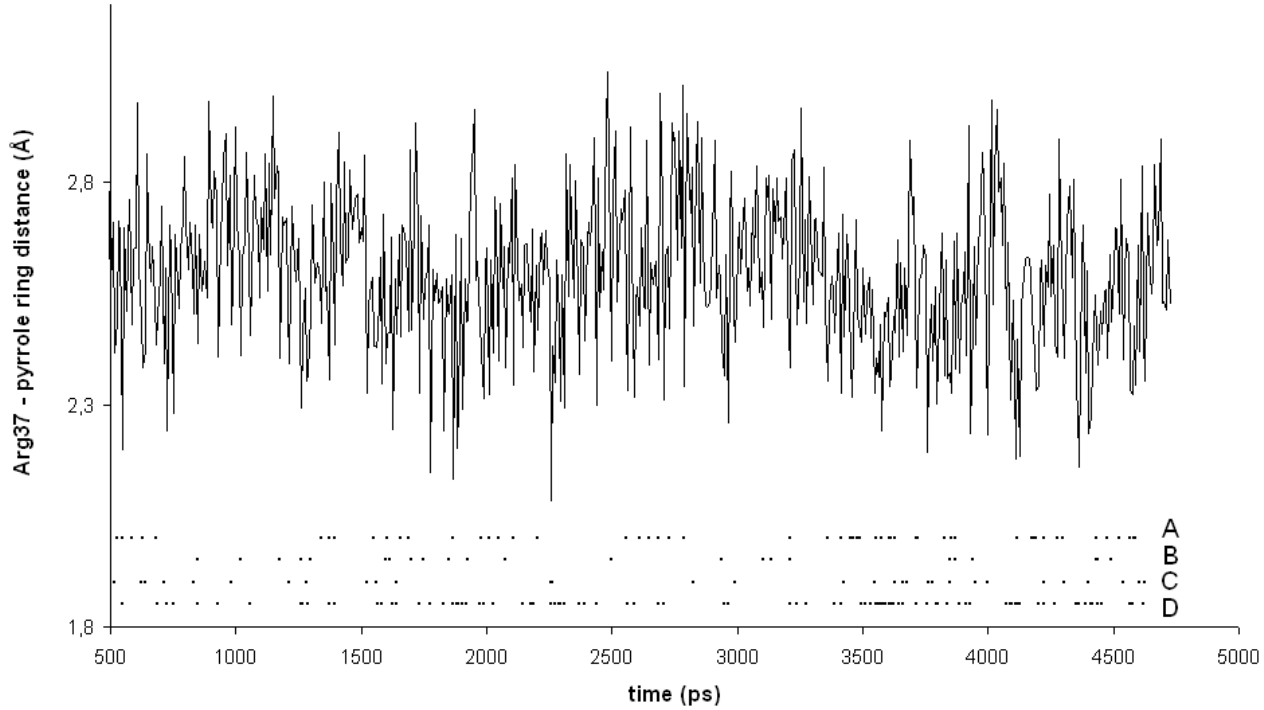

Figure 3: Minimum distance between Arg37 guanidinium protons and pyrrole C2 atoms of UroD-bound uroporphyrinogen III, as a function of simulation time. Snapshots with Arg37-C2 distances below 2.5 Å are highlighted (for each of the fours rings present in the substrate) in the lower portion of the graph. For ease of presentation, the graph only includes the first half of this simulation. Full data on this simulation, as well as simulations of Arg37 approach to the pyrrole rings in uroporphyrinogen III after sequential decarboxylation of rings D, A and B are available in the Supporting Information.

Molecular dynamics simulations of the UroD dimer allow us to analyze in more detail the overall dynamics of proton donation to the substrate by Arg37 (Figure 3). Since our previous quantum computations[4] showed that this reaction step begins with a guanidinium proton from Arg37 2.5 Å away from the pyrrole ring C2, we investigated whether in the course of the simulation Arg37 protons were able to approach within this distance of each pyrrole ring C2 atom. With intact uroporphyrinogen III, this was found to occur 37 % of the time (25.8 % for ring D, 11.0 % for ring A, 2.6 % for ring B and 4.8 % for ring C; these partial values exceed 37 % because of some overlap between the conformations close to ring A and those close to ring D). These results are consistent with the observation[14,39] that at

low substrate concentrations the first decarboxylation occurs on ring D. Simulations on D-ring-decarboxylated uroporphyrinogen III showed that without the electrostatic attraction provided by the ring D acetate group the guanidium group from Arg37 adopts an approximately equidistant position between rings A and B, so that the following decarboxylation is about as likely to occur on ring A (Arg37 approaches 80 % of the time) as on ring B (Arg37 approaches 66 % of the time). Ring C is shown to be harder to decarboxylate: after decarboxylation of rings D and A, Arg 37 approaches ring B 29.8 % of the time , *vs.* only 0.4 % of the time for ring C. Even after rings D, A and B are decarboxylated the approach of Arg37 to ring C still occurs quite intermittently (2 % of the time).

The simulation results are fully consistent with the ordered route of substrate decarboxylation observed experimentally[14,39] at low uroporphyrinogen concentrations (ring D decarboxylation, followed by rings A, B and C) and confirm our previous suggestion[4] that the proton provided by Arg37 may shuttle back and forth between the amino acid side chain and each pyrrole ring, allowing their sequential decarboxylation without the need for substrate rotation in the active site or for several rounds of substrate binding/unbinding; however, the completion of each decarboxylation requires the transfer of an additional proton to the methylene substituent arising from CO_2 release (Fig. 1). Since the enzyme must shield its active site from solvent H_3O^+, we tried to find suitable alternative proton donors for this step. Examination of the crystal structure suggested that Arg41, the amino acid lying at the entrance to the active site, might be able to provide the proton for the reactions occurring in substrate rings D and A. We found this reaction to be extremely favorable, both kinetically and thermodynamically: starting from an initial Arg41-methylene distance of 2.12 Å, a proton may be transferred to the methylene through a very early transition state (Fig. 3) lying only 2.1 kcal.mol^{-1} above the initial minimum. The reaction is exergonic by 12.6 kcal mol^{-1}, with Arg41 eventually settling 3.4 Å away from the protonated substrate. Re-protonation of Arg41 (which would allow it to transfer a new proton to the methylene formed in the reaction occurring in ring A) is expected to occur readily, since its location between the solvent and the active site allows it react with H_3O^+ without the risk of substrate side reactions.

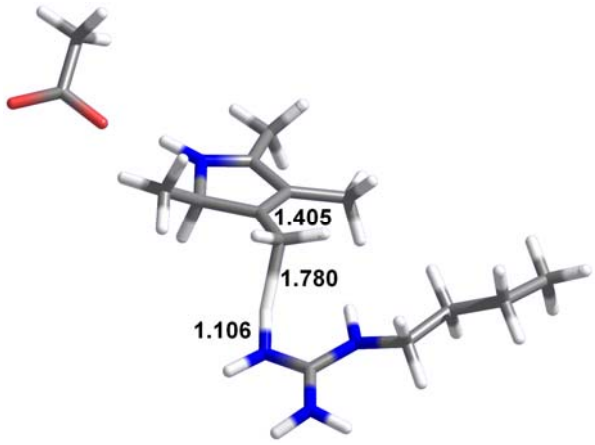

Figure 4: Structure of the transition state for proton transfer from Arg41 to the methylene substituent arising from substrate decarboxylation. All distances in Å.

Examination of the protein environment did not reveal any obvious candidates which might play a similar role regarding rings B and C of the tetrapyrrole substrate. We therefore performed molecular electrostatics calculations in order to characterize the titration behavior of the substrate-bound uroporphyrinogen decarboxylase. The results (Figure 5) clearly show that the propionic acid substituents present on rings B and C are expected to remain protonated in the physiological range. This occurs because in the binding site rings B and C are surrounded (mostly) by hydrophobic residues: the low dielectric of this region opposes the simultaneous deprotonation of the acetic acid and propionic acid substituents, since few dipoles are available to dampen the repulsion between two negatively charged centers. Decarboxylation of the acetic acid substituent removes this electrostatic interaction, so that the proton lying on the propionic acid sidechain may become available to protonate the formed methylene.

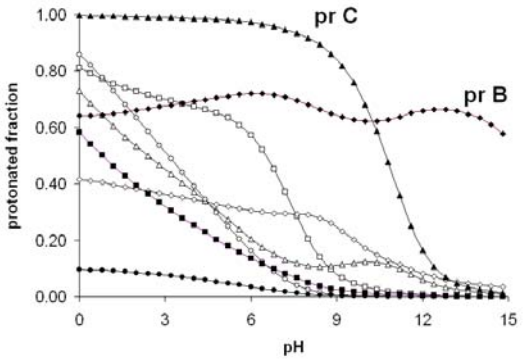

Figure 5: Titration behavior of the acetic acid (open symbols) and propionic acid (filled symbols) substituents present in uroporphyrinogen III bound to uroporphyrinogen III decarboxylase. Substituents present on ring A are depicted as squares, those on ring B as diamonds, those on ring C as triangles and those on ring D as circles.

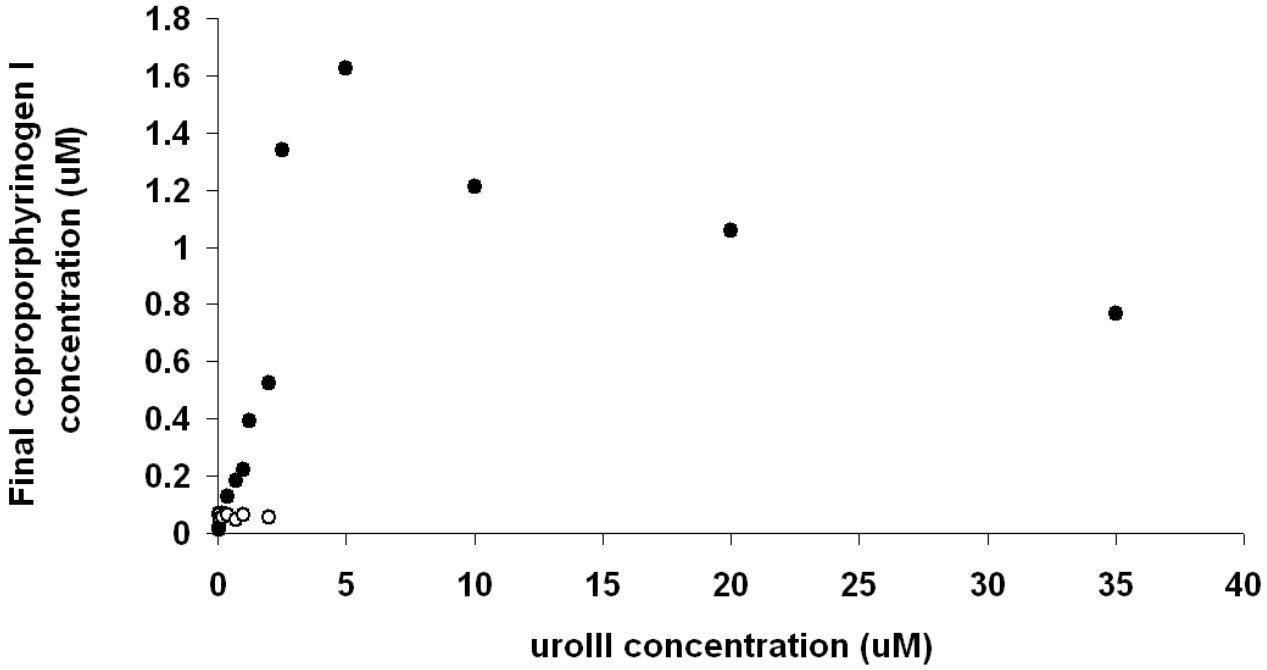

Figure 6: Activity profile of wild type (●) and R37A (○) uroporphyrinogen III decarboxylase.

The computationally-predicted roles of both Arg37 and Arg41 were further probed through site-directed mutagenesis. Four single-mutants were produced, with each of these residues substituted by either alanine or lysine. The recombinant wild type and the four modified UroD variants were produced with

an N-terminal histidine tag in *Escherichia coli* and purified in a single step by nickel – NTA chromatography as described in materials and methods. The yield of protein (from 2 to 10 mg/ml) was measured by Bicinchoninic Acid Protein Assay. Their catalytic competence was studied with 0.1 µM UroD and a large range of substrate concentrations (from 0.025 to 35 µM) in potassium phosphate buffer for 30 min at 37 °C. The amount of formed coproporphyrinogen III was analysed by HPLC chromatography (data not shown). Kinetic measurements on the wild type protein (Figure 6) showed that its reaction rate law does not fit a straightforward Michaelis-Menten form: instead of approaching a defined maximum rate as the substrate concentration is increased to infinity, we found that a maximum rate was attained at a relatively modest substrate amount (5 µM), and decreased at higher concentrations. Such an odd behavior may be explained by a kinetic model where partially decarboxylated intermediates may escape the binding site at rates competitive with the decarboxylation rate. At low substrate concentrations, these intermediates may get back inside and quickly finish conversion into coproporphyrinogen III. At higher concentrations, fresh uroporphyrinogen III competes with these intermediates for entry into the active site and prevents them from finishing conversion into coproporphyrinogen III (Figure 7). Numerical simulations of this reaction scheme confirm its ability to generate activity profiles consistent with the experimental data (Figure 8).

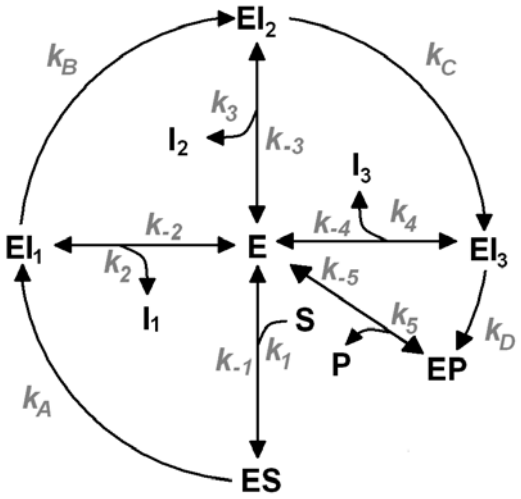

Figure 7: Proposed reaction model. E: enzyme; S: substrate; P: Product; I_n: Intermediate after *n* decarboxylations have occurred. Reaction rates of decarboxylating steps are labeled alphabetically.

Reaction rates of binding/unbinding events are labeled numerically (positive labels for binding events, negative labels for unbinding events)

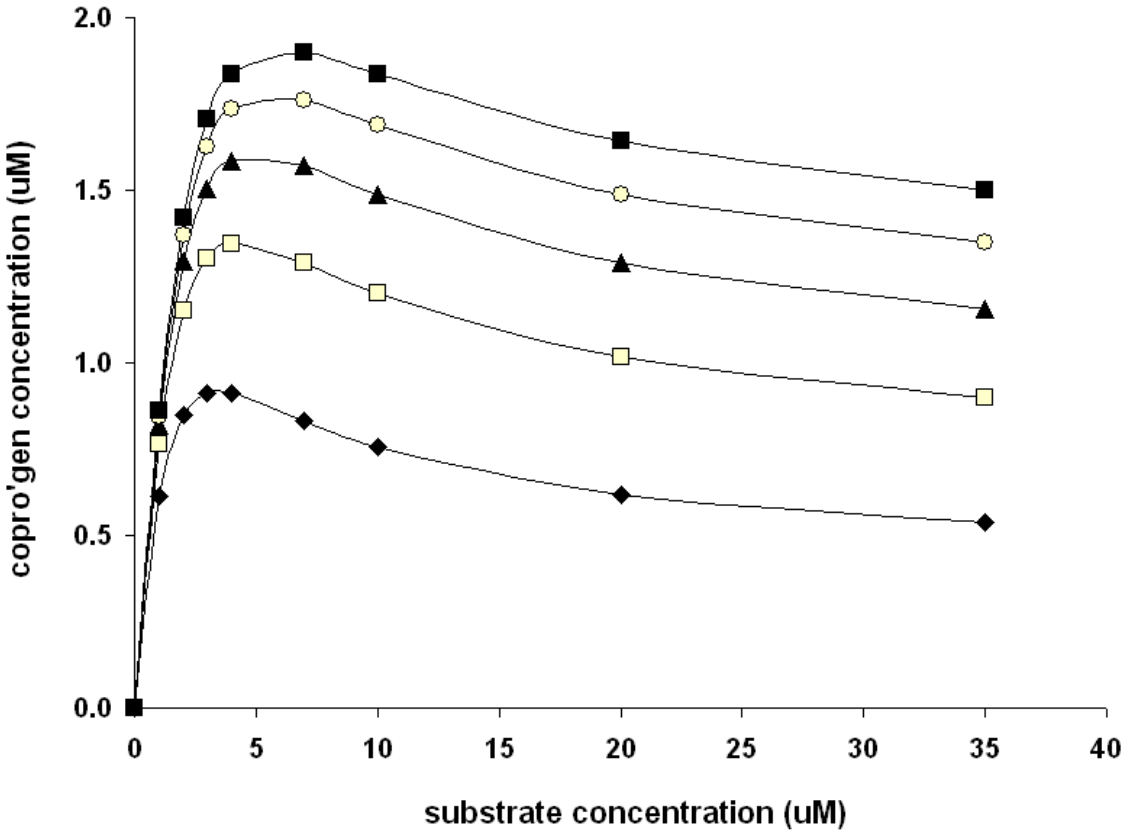

Figure 8: Kinetic profiles predicted by the reaction model depicted in Figure 7. Simulation parameters: Enzyme concentration=0.1 μmol.dm^{-3} ; Simulation time=2000 s; $k_1=k_2=k_3=k_4=k_5=10^5$ $M^{-1}s^{-1}$; $k_{-1}=k_{-2}=k_{-3}=k_{-4}=k_{-5}=0.1$ s^{-1}; $k_A=k_B=k_C=0.1$ s^{-1}; $k_D=0.02$ s^{-1} (♦) ; 0.04 s^{-1} (□); 0.06 s^{-1} (▲); 0.08 s^{-1} (○); 0.1 s^{-1} (■). Additional kinetic profiles under different parameters are available as Supporting Information

No decrease of the amount of substrate nor any reaction products could be detected upon incubation with the R37K and R41A mutants at any substrate concentrations, which clearly establishes the catalytic incompetence of these mutated enzymes. With the R37A mutant, very small amounts of coproporphyrinogen III were produced, though only at very small (0.025 to 2 μM) substrate concentrations (Figure 6). The amount of coproporphyrinogen III produced was (mostly) independent of

substrate concentration, and much smaller than observed with the wild-type enzyme. The amount of unreacted uroporphyrinogen remaining at the end of the reaction was virtually indistinguishable from the amount added initially, showing that catalysis by this mutant is not significant. In the R41K mutant, we could not detect the coproporphyrinogen III product, but non-negligible amounts of several other fluorescent products were observed.

IV Conclusions

From our computational study, the disadvantages of H_3O^+ as a general acid in this reaction become clear: although it quickly generates the protonated form of the substrate needed as an electron sink for the decarboxylation, the slow rate of decarboxylation in the presence of protonated Arg37 allows the breaking of protonated uroporphyrinogen III to become competitive with the main reaction. The use of Arg37 as a proton donor allows substrate protonation to occur, while at the same time removing the stabilizing effect of protonated Arg37 on the leaving carboxylate. Site-directed mutagenesis of this residue confirm its important role in the catalytic mechanism. The observed kinetic profile of the enzyme shows very peculiar features, consistent the release of partially decarboxylated intermediates from the acive site. The inherent flexibility of Arg37, as well as its central position in the active site, allow it to donate the catalytic proton to every pyrrole ring in uroporphyrinogen and therefore to catalyze the sequential decarboxylation of the substrate acetic acid substituents on the intact substrate and on the partially decarboxylated intermediates without the need for different binding modes for each of these species.

The computational clues pointing to the need to exclude H_3O^+ from the enzyme active site prompted the search for proton donors acting on subsequent reaction steps, which revealed the possibility of the intervention of Arg41 as an additional acid. This counter-intuitive use of two basic residues as general acids in two different proton donation steps by uroporphyrinogen decarboxylase may have arisen in evolution as an elegant solution to the problem of simultaneously binding the very negative

uroporphyrinogen (which requires a positively charged active site), and selectively protonating it while preventing excessive carboxylate stabilization by positive charges.

Supplementary Material Available: Geometries and energies of the reactants, transition states and products of all chemical reactions described. Analysis of the Arg37-pyrrole C2 distances along molecular dynamic simulations of substrate-bound and intermediate-bound UroD.

V. References

1. Wyckoff , E.E. & Kushner, J. P. (1994) Heme biosynthesis, the porphyrins and the liver. In Arias, I.m., Boyer, J.L., Fausto, N., Jakoby, W.B. Schachter, D.A. & Shafritz, D.A. (eds) *The Liver: Biology and Pathobiology*. Raven Press Ltd, New York, pp. 505-527

2. Sassa, S. & Kappas, A. (2000) *J. Intern. Med.* **247:** 169-178

3. Phillips J.D., Whitby F.G., Kushner J.P. & Hill C.P. (2003) *EMBO J.* **22**, 6225-6233

4. Silva, P.J. & Ramos, M.J. (2005) *J. Phys. Chem. B* **109:** 18195-18200.

5. Jones, R.M. & Jordan, P.M. (1993) *Biochem. J.* , **293:** 703-712

6. de Verneuil, H,. Sassa, S. & Kappas, A.(1983) *J. Biol. Chem.* **258:**2454-2460

7. Koskelo P. & Toivonen I. (1970) *Clin. Chem.* **16**, 459-461

8. Becke, A. D. *J. Chem. Phys.I*, **98** (1993), 5648.

9. Lee, C.; Yang, W.; Parr, R. J. *Phys. Rev. B*, **37** (1988), 785.

10. Hertwig, R. W.; Koch, W.; *J. Comp. Chem.*, **16** (1995), 576.

11. Siegbahn, P. E. M; Eriksson, L.; Himo, F.; Pavlov, M. *J. Phys. Chem. B.*, **102** (1998), 10622.

12. Fernandes, P. A.; Ramos, M. J. (2003) *J. Am. Chem. Soc.*, 125: 6311-6322

13. Riley K.E., Op't Holt, B.T., Merz Jr., K.M. (2007) *J. Chem. Theory Comput.,* **3**, 407-433

14. Jackson AH, Sancovich HA, Ferramola AM, Evans N, Games DE, Matlin SA, Elder GH, Smith SG. (1976) *Philos. Trans. R. Soc. Lond. B Biol. Sci.* , **273:** 191-206.

15. Barone, V.;Cossi, M. (1998) *J. Phys. Chem. A*, **102:** 1995-2001

16. Cossi, M., Rega, N, Scalmani, G., Barone, V. (2003) *J. Comput. Chem.* 24: 669

17. M. J. Frisch, G. W. Trucks, H. B. Schlegel, G. E. Scuseria, M. A. Robb, J. R. Cheeseman, J. A. Montgomery, Jr., T. Vreven, K. N. Kudin, J. C. Burant, J. M. Millam, S. S. Iyengar, J. Tomasi, V. Barone, B. Mennucci, M. Cossi, G. Scalmani, N. Rega, G. A. Petersson, H. Nakatsuji, M. Hada, M. Ehara, K. Toyota, R. Fukuda, J. Hasegawa, M. Ishida, T. Nakajima, Y. Honda, O. Kitao, H. Nakai, M. Klene, X. Li, J. E. Knox, H. P. Hratchian, J. B. Cross, C. Adamo, J. Jaramillo, R. Gomperts, R. E. Stratmann, O. Yazyev, A. J. Austin, R. Cammi, C. Pomelli, J. W. Ochterski, P. Y. Ayala, K. Morokuma, G. A. Voth, P. Salvador, J. J. Dannenberg, V. G. Zakrzewski, S. Dapprich, A. D. Daniels, M. C. Strain, O. Farkas, D. K. Malick, A. D. Rabuck, K. Raghavachari, J. B. Foresman, J. V. Ortiz, Q. Cui, A. G. Baboul, S. Clifford, J. Cioslowski, B. B. Stefanov, G. Liu, A. Liashenko, P. Piskorz, I. Komaromi, R. L. Martin, D. J. Fox, T. Keith, M. A. Al-Laham, C. Y. Peng, A. Nanayakkara, M. Challacombe, P. M. W. Gill, B. Johnson, W. Chen, M. W. Wong, C. Gonzalez, and J. A. Pople, Gaussian 03, Revision B.04, Gaussian, Inc., Pittsburgh PA, 2003.

18. Blomberg, M. R. A.; Siegbahn, P. E. M.; Babcock, G. T. (1998) *J. Am. Chem. Soc.*, **120**, 8812.

19. Mulliken, R. S. (1955) *J. Chem. Phys.* **23**, 1833

20. Bashford, D.; Gerwert. K. (1992) *J. Mol. Biol.* **224**, 473-486

21. Sitkoff, D; Sharp, K.A.; Honig, B (1994) *J. Phys. Chem.*, **98**, 1978-1988

22. Whitby FG, Phillips JD, Kushner JP, Hill CP (1998) *EMBO J.*, **17**, 2463-2471

23. Dolinsky TJ, Nielsen JE, McCammon JA, Baker NA. (2004) *Nucl. Acids Res.*, **32,** W665-W667

24. Martel, P.J.; Soares, C.M.; Baptista, A.M.; Fuxreiter, M.; Náray-Szabó, G.; Louro, R.O.; Carrondo, M.A. (1999) *J. Biol. Inorg. Chem.*, **4**, 73-86

25. Antosiewicz, J.; McCammon, J.A.; Gilson, M.K. (1994) *J. Mol. Biol.*, **238**, 415-436

26. Gilson, M. K.; Sharp, K.A.; Honig B. (1988) *J. Comput. Chem.*, **9**, 327-335.

27. Baptista, A.M.; Martel, P.J., Soares, C.M. (1999) *Biophys. J.*, **76**, 2978-2998

28. Teixeira, V.H.; Soares, C.M.; Baptista, A.M. (2002) *J. Biol. Inorg. Chem.*, **7**, 200-216

29. Krieger E, Darden T, Nabuurs S, Finkelstein A, Vriend G (2004) *Proteins* **57**,678-683

30. Wang J, Cieplak P, Kollman PA (2000) *J. Comput. Chem.* **21**,1049-1074

31. Essmann U, Perera L, Berkowitz ML, Darden T, Lee H, Pedersen LG (1995) *J Chem Phys* 1995; **103**, 8577-8593.

32. Berendsen HJC, Postma JPM, van Gunsteren WF, DiNola A, Haak JR. (1984) *J. Chem. Phys.* **81**, 3684-3690.

33. Jakalian A, Jack DB and Bayly CI (2002) *J. Comput. Chem.* **23**,1623-1641

34. Krieger E, Nielsen JE, Spronk CA, Vriend G (2006) *J. Mol. Graph. Model.* **25**, 481-486

35. Phillips, J. D., Whitby, F. G., Kushner, J. P. & Hill, C. P. (1997) *Protein Sci.* **6**, 1343-1346.

36. Romeis, B. (1968) Mikroskopische Technik (16. Aufl.) p. 593 (R. Oldenbourg Verlag, München).

37. Phillips, J. D. & Kushner, J. P. (1999) *Current Protocols in Toxicology*, 8.4.1-8.4.13.

38. Silva, P.J; Ramos, M.J. (2008) *J. Phys. Chem. B*, **112**, 3144-3148

39. Lash, T.D.; Mani, U.N.; Lyons, E.A.; Thientanavanich, P.; Jones, M.A.(1999) *J. Org. Chem.*, **64**, 478-487